Materiales

Revista Mexicana de Ingeniería Química

SYNTHESIS AND CHARACTERIZATION OF CALCIUM PHOSPHATE NANOPARTICLES AND EFFECT OF THE AGITATION TYPE ON PARTICLES MORPHOLOGY

SÍNTESIS Y CARACTERIZACIÓN DE NANOPARTÍCULAS DE FOSFATO CALCICO Y EFECTO DEL TIPO DE AGITACIÓN EN LA MORFOLOGÍA DE LAS PARTÍCULAS

E.A. Flores-Hernández[1], R.H. Lira-Saldívar[2*], R. Acosta-Ortiz[2], B. Méndez-Arguello[3], J.I. García-López[4], E. Díaz-Barriga-Castro[2], A. González-Torres[1], M. García-Carrillo[1]

[1]*Universidad Autónoma Agraria Antonio Narro Unidad Laguna (UAAAN-UL). Periférico Raúl López Sánchez S/N, Col. Valle Verde. C.P. 27054. Torreón, Coahuila. México.*

[2]*Centro de Investigación en Química Aplicada (CIQA), Blvd. Enrique Reyna Hermosillo No.140 C.P. 25294. Saltillo, Coahuila. México.*

[3]*Universidad Intercultural del Estado de Puebla. Calle Principal a Lipuntuahuaca S/N, Lipuntahuaca, Huehuetla, Puebla, México.*

[4]*Laboratorio de Química y Bioquímica, Facultad de Agronomía, Universidad Autónoma de Nuevo León, General Escobedo, Nuevo León C.P. 66050, México*

Abstract

This paper reports a rapid, economic and efficient process to prepare calcium phosphate nanoparticles (nCF), also known as hydroxyapatite. The objective of this study was to synthesize, characterize and determine the effect of agitation type on production and morphology of nCF. Synthesis was carried out by wet chemical precipitation, with mechanical and magnetic agitation. TEM microscopy indicates that mechanical agitation produced ∼ 27% particles with diameter between 15-20 nm, while magnetic stirring formed 31.1%. The sizes range obtained for both agitations types was 10 to 45 nm, with the predominant size being 15 to 20 nm. The FTIR spectrometry analysis revealed that the nCF obtained are analogous to those reported in the literature. Zeta potential values of -20 mV to -14 mV were obtained for mechanical and magnetic agitation respectively, suggesting that nCF synthesized by mechanical agitation has greater electrostatic repulsion in aqueous suspension. The results obtained reveal that mechanical stirring improves the nanocomposite characteristics and produce colloidal particles more stable in aqueous suspension. We consider that the process reported here could be scalable to produce nCF, which has commercial potential as a nanofertilizer for agricultural use.

Keywords: characterization, morphology, nanoparticles, hydroxyapatite.

Resumen

Este artículo reporta un proceso rápido, económico y eficiente para preparar nanopartículas de fosfato de calcio (nFC), también conocida como hidroxiapatita. El objetivo de este estudio fue sintetizar, caracterizar y determinar el efecto del tipo de agitación en la producción y morfología de las nFC. La síntesis se realizó mediante precipitación química húmeda, con agitación mecánica y magnética. La microscopía TEM indica que la agitación mecánica produjo ∼ 27% de partículas con un diámetro entre 15-20 nm, mientras que la agitación magnética produjo 31.1%. El rango de tamaños obtenidos para ambos tipos de agitación fue de 10 a 45 nm, con un tamaño predominante de 15 a 20 nm. El análisis de espectrometría FTIR reveló que las nFC obtenidas son análogas a las reportadas en la literatura. Se obtuvieron valores de potencial Zeta de -20 mV a -14 mV para la agitación mecánica y magnética respectivamente, esto sugiere que las nFC sintetizadas por agitación mecánica son más estables en suspensión. Los resultados revelan que la agitación mecánica mejora las características del nanocompuesto y produce partículas coloidales más estables en suspensión acuosa. Consideramos que el proceso aquí descrito podría ser escalable para producir nFC, que pudiese tener potencial comercial como nanofertilizante para uso agrícola.

Palabras clave: caracterización, morfología, nanopartículas, hidroxiapatita.

1   Introduction

The interdisciplinary research on biosystems at nanoscale involves physical sciences, chemical and molecular engineering, biology, biotechnology, medicine and agronomy (Ferreira and Filipe, 2018), complementing in this way the knowledge required for the synthesis of new products and agro-inputs, which are used in food systems (Prakash *et al.*, 2018), regenerative medicine (Yang *et al.*, 2019) and in the development of new intelligent textiles (Asif and Hasan, 2018), among many other applications. The synthesis and use of metallic, mineral and carbon-derived nanoparticles (NPs) represent a very attractive and promising area, because of the potential impact on current and future society.

It has been pointed out that hydroxyapatite NPs (HA, $Ca_{10}(PO_4)_6(OH)_2$) (Figure 1) also known as calcium nanophosphate (nCF), it is considered as one of the most prominent materials for therapeutic applications, and owing to its phosphorus (P) and calcium (Ca) content, it has a promissory potential as fertilizer in agriculture, although the latter possibility still needs many studies and validation in the field (Kottegoda *et al.*, 2017). One of the main applications of HA NPs is in the biomedical area, since they can be used in therapy and transport of genes, for bone repair treatment, as well as in acquired and inherited diseases
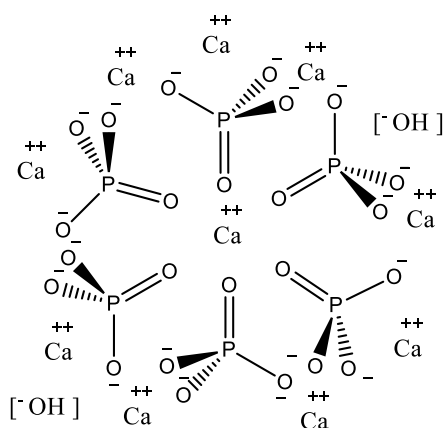

Fig. 1. Chemical structure of a molecule of hydroxyapatite also known as calcium phosphate, mainly formed by crystalline calcium phosphate, being the main inorganic component of bones in vertebrates.

(Bakan, 2018). Salgado-Delgado *et al.* (2016) reported that poly (2-hydroxyethyl methacrylate) and chitosan were combined to obtain a biocomposite material with fillers of hydroxyapatite through foaming gas effect. Their results obtained by SEM indicate a biocomposite formation having high porosity, with an interpenetrated network in the porous material, which could be used for medical applications.

Other important uses of nCF are in water treatment and remediation of soils polluted with heavy metals (Sadat *et al.*, 2013). Mendoza-Castillo *et al.* (2016), stated that the use of bone char which contains hydroxyapatite, could be considered as alternative sorbent for treatments of aqueous solutions polluted by Cd^{2+}, Ni^{2+} and Zn^{2+}. It has also been documented that this type of NPs can increase the vitality of *Zea mays* plants by improving the content and production of chlorophyll, increasing the growth of plants and the proliferation of roots, so that this type of NPs could be used as high efficiency nanofertilizers (Rane *et al.*, 2015).

In many regions of Mexico as in other countries with agricultural vocation, the efficient use of fertilizers is highly demanded to optimize the cost of crops production, to make a sustainable use of inputs and to reduce contamination of agroecosystems (Bationo *et al.*, 2018). Between 50-70% of nitrogen (N) applied to the soil as conventional fertilizer is lost due to leaching and volatilization such as ammonia and N oxides (Kottegoda *et al.*, 2011). In acidic and alkaline soils that make up more than 70% of the world's arable land, P forms insoluble compounds; in acidic soils it forms phosphates of Al and Fe, while in alkaline soils it forms phosphates of Ca and Mg, all of them with low solubility (Holford, 1997), that are not available to plants, therefore, up to 80% of the applied P is lost because it becomes immobile and unusable for crops (Lopez-Bucio *et al.*, 2000).

Therefore, nanotechnology (NT) as a tool to formulate nanopesticides and nanofertilizers offers a significant improvement for the efficient use of this costly and important agro-input. Montalvo *et al.* (2015) carried out a work where nCF was used as phosphorous fertilizer; they performed an assay using the technique of P isotope dilution, to quantify the absorption of P by plants of *Triticum aestivum* from nCF, calcium phosphate (CF) and triple superphosphate, applied to different types of soils. The results showed that P release and solubility was higher with nCF.

Scientific literature accounts with numerous publications referring to the most common procedures

to obtain nCF. Sadat *et al.* (2013) made a classification of five main methods: 1) dry processes, 2) wet processes, 3) high temperature processes, 4) synthesis from biological sources and 5) a combination of these procedures. It is considered that the conventional wet precipitation process is the simplest, easier and most popular to use (Kottegoda *et al.*, 2011), due to insolubility of nCF in water (Guzmán *et al.*, 2005). The conditions for these reactions are easily controllable and versatile with economic advantages like cost-effective on industrial scale, reproducibility and the fact that not require expensive equipment, because by mixing two aqueous solutions results in the formation of highly supersaturated solutions of nCF, which induces rapid precipitation of nanoparticles (Angelescu *et al.*, 2011; Okada and Matsumoto, 2015).

Thus, the objective of this work was to evaluate a simple and economic chemical process that produce the highest amount of nCF powders, considering that in the medium term this technique could be used for the commercial production of nanofertilizers.

2 Materials and methods

2.1 Materials and equipment

The following reagents were used: phosphoric acid (H_3PO_4, 85%), calcium hydroxide [Ca (OH)$_2 \geq 95\%$] and ammonium hydroxide (NH$_4$OH $\geq 85\%$), were of analytical grade (Jalmek brand). The employed laboratory equipment was: IKA brand digital helical agitator model RW 20; a magnetic stirrer with heating, Thermo Scientific brand; an electric heating mantles for ball flask; a condenser with recirculating bath and a potentiometer Thermo Scientific model Orion Star A211.

2.2 Synthesis of calcium phosphate nanoparticles (nCF)

The synthesis of nCF was carried out with a procedure similar to that described by Guzmán *et al.* (2005), which consisted on performing forced mechanical agitation at 1,000 rpm, repeating the procedure and applying magnetic stirring with a speed of 1,200 rpm. An aqueous solution of calcium hydroxide [Ca(OH)$_2$] and orthophosphoric acid (H_3PO_4) was used, with a stoichiometric Ca / P ratio of 1.67 (Yelten and Yilmaz, 2016), adjusting the final pH to 11.74 by means of a ammonium hydroxide solution. Subsequently the

mixture was kept in constant agitation and heated to 95 ° C in order to activate the chemical reaction, which was executed according to the following equation:

$$6H_3PO_4 + 10Ca(OH)_2 \rightarrow Ca_{10}(PO_4)_6(OH)_2 + 18H_2O \quad (1)$$
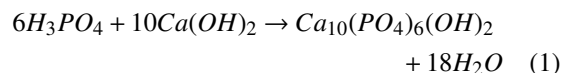
Once the nCF synthesis reaction was carried out, the resulting solution was allowed to stand for 72 h until the expected product was precipitated, observing the phase separation at the end of the indicated time. This was performed by making a modification to the procedure indicated by Guzmán *et al.* (2005), by eliminating the supernatant by decantation. Subsequently, the precipitate was dried for 72 h at 110 °C.

2.3 Characterization by infrared spectroscopy and Fourier transforms (FTIR)

The nCF samples were characterized by Fourier transform infrared spectroscopy (FTIR) technique, recorded in a Thermo Scientific infrared spectrometer model Nicolet 6700, and using the KBr disc technique.

2.4 Characterization by X-ray diffraction (XRD)

An XRD Rigaku Ultima IV diffractometer with KαCu radiation (1.54183 Å) was used to analyze nCF samples. The XRD diffraction patterns were recorded in a 2θ range of 10 to 80 ° with the minimum step size of 0.02 ° and with a sweep of 5 °/min. The calculation to obtain the average size of crystallite particles, was carried out by means of the Halder-Wagner method (Izumi and Takuji, 2015) and the software installed in the diffractometer employed.

2.5 Characterization by transmission electron microscope (TEM)

The samples morphology and microstructure was determined by using a FEI-TITAN 80-300 kV microscope operated at an acceleration voltage of 300 kV. The samples for these analyses were prepared by depositing and evaporating a drop of the colloidal solution on lacey carbon copper grids. The processing of TEM micrographs, were interpreted using the Digital Micrograph 3.7.0 software (Gatan Software, Inc., Pleaston, CA, USA). nCF description was performed with a transmission electron microscopy images and high resolution (TEM and HRTEM), as well by electron diffraction (SAED).

2.6 Characterization by Zeta potential (ZP)

In the present study ZP was determined using a ZETA-check micro trac equipment from Colloid Metrix Company and a microscope to observe the colloidal particles inside a chamber or electrophoretic cell. ZP determines the surface charge of nanoparticles when measuring their electrical potential, which can be affected by particle composition and the medium in which it is dispersed (Velasco *et al.*, 2012). This variable represents the amount of repulsion or electrostatic attraction (or charge) between nCF particles and other particles. It is one of the important parameters that affect the stability of a suspension (Saxena and Okram, 2018). The measurement of this parameter provides detailed information on the causes for dispersion, aggregation or flocculation, and can be applied to improve the formulation of dispersions, emulsions and suspensions (Mikolajczyk *et al.*, 2015).

3 Results

3.1 Synthesis of calcium phosphate nanoparticles

nCFs were obtained by means of mechanical and magnetic agitation with an average size between 10 to 45 nm (Figure 2). These dimensions are within the desirable range for biomedical applications, mainly for bone tissue applications (Sunandhakumari *et al.*, 2018; Sattary *et al.*, 2019) and for their study and practice in agriculture (Kottegoda *et al.*, 2017).

3.2 Characterization of calcium phosphate nanoparticles

Figure 3 shows the FTIR spectrum obtained from the nCF sample obtained by mechanical agitation. Typical bands were observed for this mineral, identical to those reported in the literature (Ma, 2012; Gheisari *et al.*, 2015). A main band centered at 1060 cm^{-1} is appreciated as well as other bands centered at 964, 606 and 573 cm^{-1} respectively, which are distinctive of the phosphate groups. The narrow band at 3571 cm^{-1} is attributed to the stretch vibration of the hydroxyl groups. The wide band centered at 3430 cm^{-1} together with the signal at 1639 cm^{-1}, indicate the presence of adsorbed water on the nCF surface, while the signals at 1456 cm^{-1} and 1424 cm^{-1} correspond to carbon dioxide, which is also adsorbed on the NPs surface. The spectrum of the magnetically stirred sample displayed an identical FTIR spectrum to that obtained by mechanical stirring.
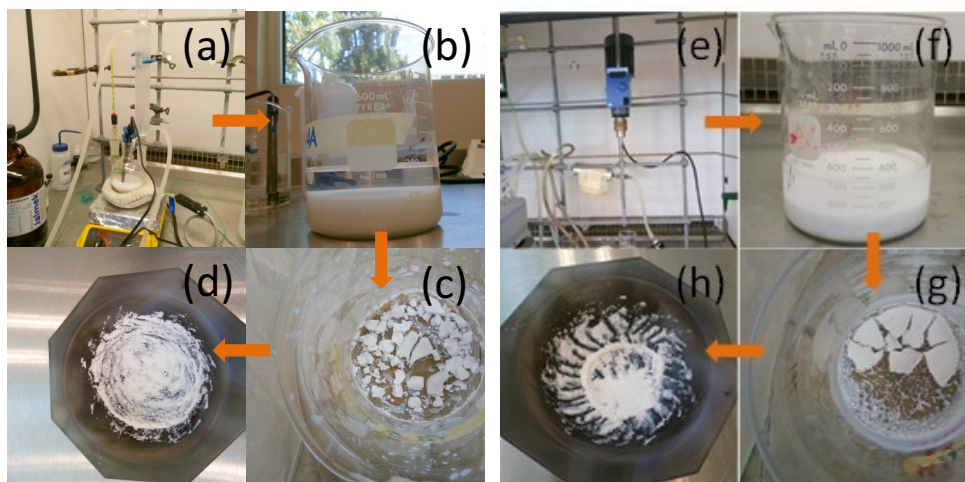

Fig. 2. Process for the synthesis of nCF NPs (a) and (e) arrangement of laboratory instruments for the synthesis reaction by magnetic and mechanical agitation respectively. (b) and (f) solution obtained after the reaction by both types of agitation. (c) and (g) product obtained after drying for magnetic and mechanical stirring respectively. (d) and (h) reduction of particle size.
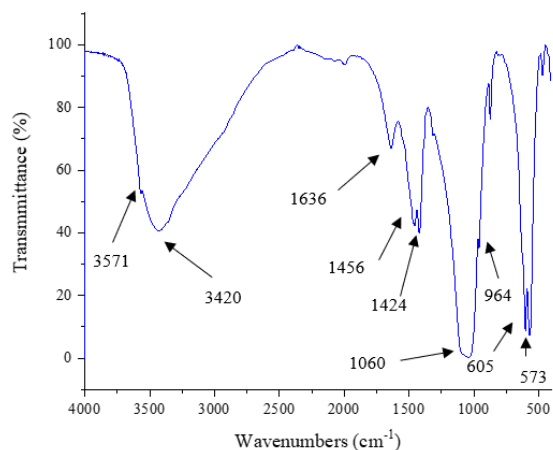
Fig. 3. Fourier transform infrared transmission spectroscopy (FTIR) of the calcium phosphate sample obtained by the mechanical agitation technique.
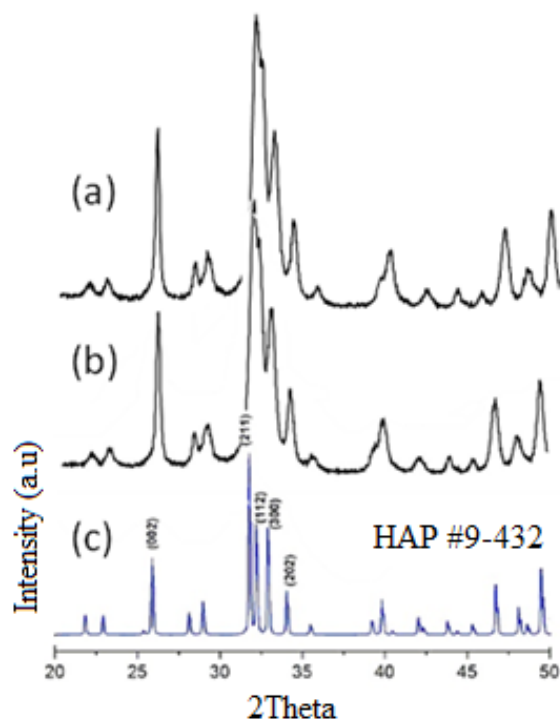

Fig. 4. XRD diffraction patterns of the nCF NPs powder sample obtained by: (a) Magnetic stirring, (b) Mechanical stirring and (c) Standard diffraction pattern for FC according to JCDPS letter 9-432.

Figures 4 (a) and 4 (b) shows the X-ray diffraction patterns of the precipitate obtained by means of non-calcined wet chemical synthesis and using magnetic and mechanical agitation. The obtained results agree with typical responses with greater intensity in the

peaks (002, 211, 112, 300 and 202), characterizing this powder as a pure calcium phosphate, according to the international data base JCDPS 9-432, as shows in Figure 4 (c), thus confirming the formation of nCF.

Our results show that the agitation type and the speed applied did not cause a significant difference on size of crystallite produced, since the average size for the magnetic stirring was 10.9 ± 1.1 nm, while by means of mechanical agitation the average size was 15.2 ± 1.3 nm, a difference of 6.7 nm (28.28% larger size) was attained by means of mechanical agitation. The NPs size distribution is presented in Figures 5 (a) and 5 (b).

In order to evaluate the previous results, a sample analysis was carried out using the TEM microscope, Figure 6 (a) depicts the TEM image of an nCF synthesized with mechanical agitation. In this micrograph an elongated rod shape of NPs is observed. Figure 6 (b) shows the distribution of nCF sizes after measuring 350 nanoparticles. The majority ($\sim 65\%$) of NPs displayed diameters of 10 to 25 nm, but only $\sim 4\%$ exhibited sizes greater than 35 nm. Figure 6 (c) shows a representative image of HRTEM, where the molecule diameter with a mean value of 29.26 nm is clearly appreciated. This outcome agrees with the average size frequency observed in the scheme of panel 6 (b). The SAED diffraction pattern obtained from the area observed in panel (a), is shown in Figure 6 (d). This pattern is made up of irregular rings associated with the planes (211, 102, 201 and 200) of the structure of nCF.

Dimension measurements were made by triplicate for each type of agitation employed. The image analysis to determine main diameter of each process was performed using TEM images of the three replicates by measuring at least the 350 nanoparticles each time. For FTIR, XRD and ZP analyzes, there were no differences between analyses, and therefore, only one of the results is reported here. To determine the particle size distribution from the CTEM images, the following procedure was performed: 1) Using the Image Pro 10 software, mean diameter of 350 NPs was measured for each agitation method. 2) From the obtained data, the absolute frequency for typical diameter ranges was determined. 3) With the above data expressed as a percentage the histograms created and are presented on Fig. 6 (b) and Fig. 7 (b).

Figure 7 (a) is a conventional TEM micrograph corresponding to the nCF magnetically stirred sample, in which the quasi-spherical morphology is clearly visible. Figure 7 (b) shows the size distribution that resulted after measuring 350 nanoparticles.
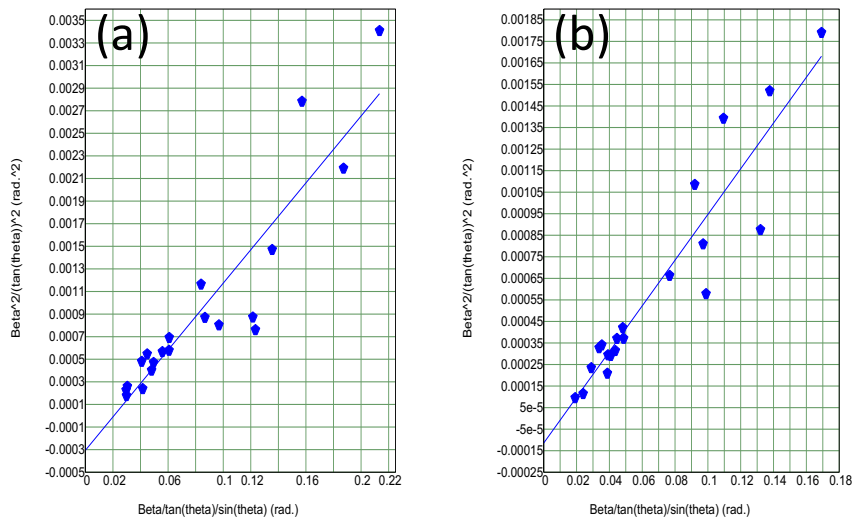
Fig. 5. Graphs of crystallite size distribution achieved by the Halder-Wagner method, and obtained by wet chemical reaction and magnetic (a) and mechanical (b) agitation.
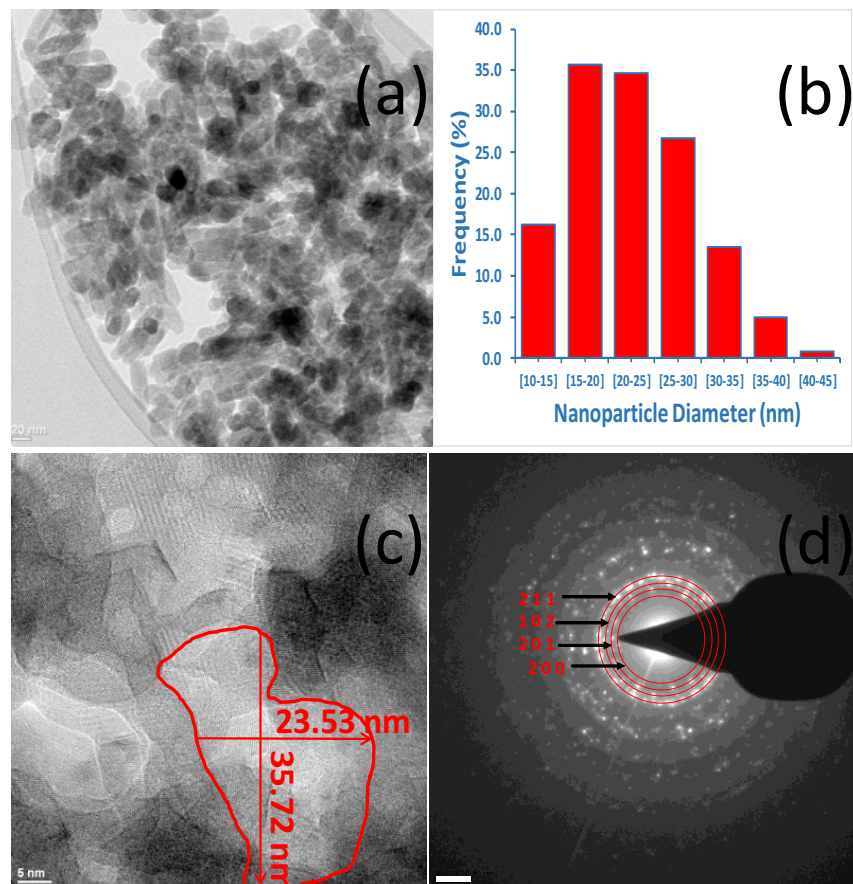

Fig. 6. Micrographs corresponding to the nCF sample obtained by mechanical agitation. Image of TEM (a). Distribution of the size of NPs (b). HRTEM image of a nanoparticle (c). SAED diffraction pattern obtained from the area observed in the panel (d).
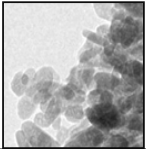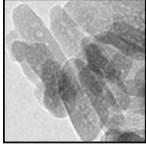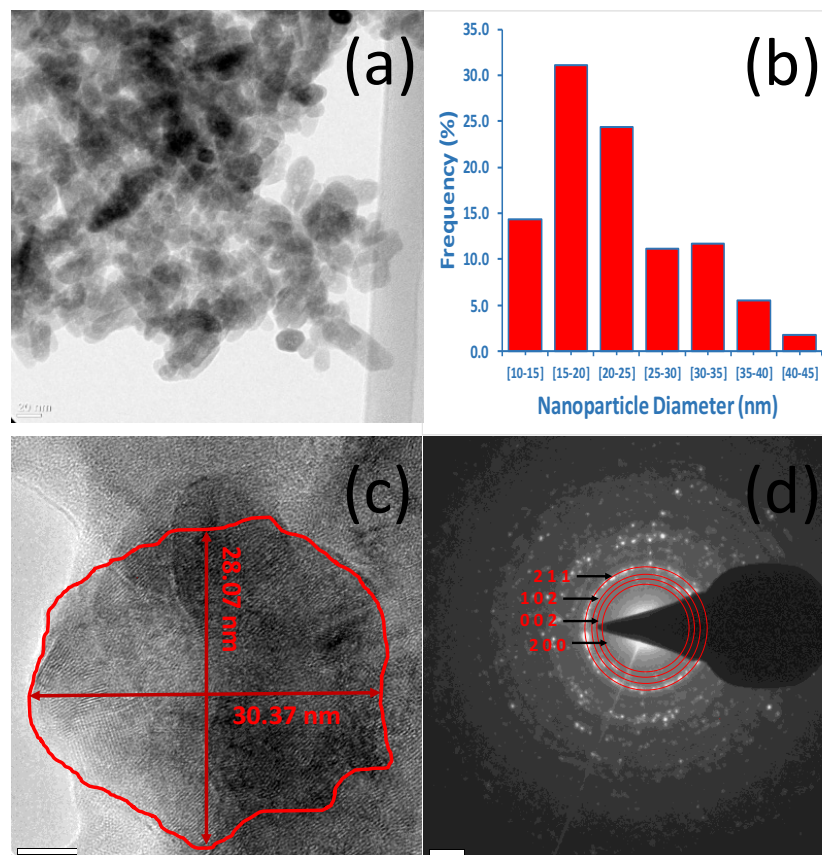
Fig. 7. Micrographs corresponding to the nCF sample obtained by magnetic agitation. (a) TEM image (a). Distribution of the size of NPs (b). HRTEM image of a nanoparticle (c). SAED diffraction pattern obtained from the area observed in panel (b).

Table 1. Effect of mechanical and magnetic stirring on some characteristics related to nanophosphate calcium synthesized, such as diameter range, number of particles per diameter range, average size and statistical parameters.

	Mechanical stirring / Magnetic stirring				
Diameter range of NPs (nm)	Number of Particles by diameter	Particles average size	Standard deviation	Standard error	Variability coeficient
10-15	43 / 49	13.26 / 13.23	1.27 / 1.54	0.19 / 0.22	9.57 / 11.66
15-20	95 / 106	17.7 / 17.55	1.41 / 1.36	0.14 / 0.13	7.98 / 7.77
20-25	92 / 83	22.84 / 22.33	1.34 / 1.39	0.14 / 0.15	5.88 / 6.23
25-30	71 / 38	27.44 / 27.36	1.55 / 1.46	0.18 / 0.24	5.66 / 5.34
30-35	36 / 40	32.2 /32.64	1.32 / 1.48	0.22 / 0.23	4.11 / 4.53
35-40	13 / 19	37.17 / 37.61	1.27 / 1.62	0.35 / 0.37	3.42 / 4.31
40-45	2 / 6	42.32 / 42.05	2.84 / 1.75	2.01 / 0.71	6.71 / 4.15

Table 2. Nanophosphate calcium characteristics related to morphology, yield, and ZP based on the employed agitation type.

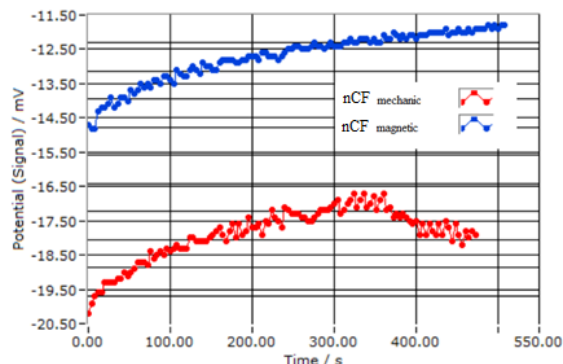| Type of agitation and nCF shape	nCF morphology	Yield (g/L)	Z Potential (mV)
Magnetic agitation (quasi spherical shape)		100	-14.5
Mechanical agitation (rod shape)		100	-20.0

Fig. 8. Zeta potential illustrating the electrical potential related to the dispersion of the aqueous suspension of the calcium phosphate nanoparticles, which were obtained by mechanical agitation and magnetic stirring.

Most NPs ($\sim$ 70%) displayed average diameters from 10-25 nm, and only $\sim$ 7% exhibited sizes greater than 35 nm. Figure 7 (c) is a representative image of HRTEM, where an average diameter of 29.22 nm is observed. Figure 7 (d) reveals the SAED diffraction pattern obtained from the area observed in panel (a), revealing that the pattern is made up of irregular rings associated with the planes (211, 102, 002 and 200) of the nCF structure.

Table 1 shows the comparative data resulting from measurements of nCF diameters obtained by two agitation types employed for the production of nCF by wet chemical precipitation method. Table 2 displays some morphological characteristics like average size and estimated yield for each agitation type. The ZP value as a function of time and the two types of agitation used for the synthesis of the nCF is presented in Figure 8. The results show values of up to -20 mV (millivolts), but with a tendency toward zero with increasing time.

Regarding the morphology of the nanoparticles, there is a noticeable difference between the types of agitation employed, since the cuasi spherical and rod shapes obtained depended on the stirring method. In the case of mechanical agitation mostly prevailed a shaped rod nanoparticles, while the magnetic stirring made almost spherical shapes, having a size between 15 and 25 nm; which is in agreement with Alvear *et al.* (2017), since these authors also reported that agitation speed in the case of mechanical agitation induced smaller particle sizes (Fig. 8.)

Table 3 shows the economical features associated to produce 1 kg of nCF by three different methods, taking into account only the expenses for ACS grade reagents, according to local suppliers' quotation, leaving aside other collateral expenses such as laboratory equipment, time of process, as well as electric energy used. The nCF synthesis processes analyzed were wet chemical precipitation, sol-gel and dry method. The specific reactions for each synthesis methods are presented as follows:

Reactions for wet chemical precipitation according to Guzmán *et al.* (2005):

$$6H_3PO_4 + 10Ca(OH)_2 \rightarrow Ca_{10}(PO_4)_6(OH)_2 + 18H_2O \quad (2)$$

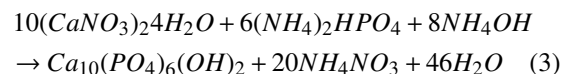$$10(CaNO_3)_2 4H_2O + 6(NH_4)_2HPO_4 + 8NH_4OH \rightarrow Ca_{10}(PO_4)_6(OH)_2 + 20NH_4NO_3 + 46H_2O \quad (3)$$
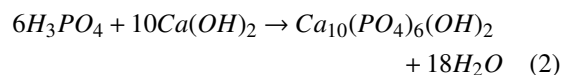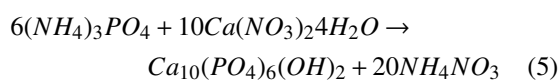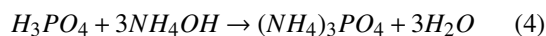
Table 3. Amount (pesos) necessary to produce 1 kg of nanophosphate calcium by using three different methods.

Synthesis method	Amount to produce 1 kg
Wet precipitate according to equation 1	$812.68
Wet precipitate according to equation 2	$2,685.00
Sol - gel employing equations 3 and 4	$1,824.96
Dry method employing equation 5	$3,832.93

Reactions for the sol-gel synthesis method according to Sanosh *et al.* (2009):

$$H_3PO_4 + 3NH_4OH \rightarrow (NH_4)_3PO_4 + 3H_2O \quad (4)$$

$$6(NH_4)_3PO_4 + 10Ca(NO_3)_2 4H_2O \rightarrow$$
$$Ca_{10}(PO_4)_6(OH)_2 + 20NH_4NO_3 \quad (5)$$

The last two reactions are consecutive, since they belong to the same method.

Reaction required for the dry method according to Fihri *et al.* (2017):

$$3Ca_3(PO_4)_2 + 3CaO \rightarrow Ca_{10}(PO_4)_6(OH)_2 \quad (6)$$
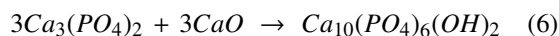
In the previous comparison it is clear that the most economical option turns out to be equation one (synthesis by wet chemical precipitation), however, for the eventual case that this nanoparticle is oriented to commercial application, a lower price will be necessary, so the production cost needs to be recalculated but using industrial grade reagents. By doing so, a decrease of 89.4% is achieved. In this way the nCF production cost will be $ 85.90 / kg. This relative low price is in agreement with many agro inputs used as soil amendment or soil fertilizer.

4 Discussion

The results of this work agree with previous reports where the particle size of nCF is closely related to the speed of agitation during the reaction, for instance Afshar *et al.* (2003) pointed out that it is best to perform a powerful and high-speed mechanical agitation, therefore, the speed of agitation during the wet chemical synthesis reaction is a critical step in that process and has an impact on the performance of the reaction. In an analogous way, Azizieh *et al.* (2011) reported that by increasing the rotational speed, as a result of greater heat input, the grain size of the base alloy increased and simultaneously more shattering effect of rotation was observed, causing a better nanoparticle distribution.

When performing the synthesis of magnetite NPs, Alvear *et al.* (2017) established a directly proportional relationship between the yield and the agitation speed of the reaction. Their results indicate that the production of Fe_3O_4 NPs occurs in accordance with the theory of nucleation and crystal growth, showing that increasing the speed of agitation rises the nucleation speed, and consequently the reaction performance. These authors also mention that a high speed of agitation tends to obtain smaller and more uniform particles, as it happened in the present work when performing the synthesis of the nCF. In this way it was demonstrated that the 1000 rpm agitation speed generated the maximum yield for both stirring types, and better uniformity in NPs size with average diameters of 15-20 nm.

In relation to the aforementioned, Salimi *et al.* (2012) studied the effect of agitation speed, type of agitation and temperature, on the size and morphology of nCF, but using the sol-gel technique. They found that by increasing the force of agitation, the dissipation energy of the system was increased, generating great turbulence in the mixing zone and increasing the nucleation rate, in addition, the large aggregates were fractionated. These results coincide with those obtained in the present work regarding particle size, since the mechanical agitation produced $\sim$ 33% of particles with a diameter between 15-20 nm, while the magnetic agitation produced 29%. The range of particle sizes obtained for both types of agitation was 10 to 45 nm, however, the predominant size was 15 to 20 nm.

The present study reveals that nCF synthesis of by mechanical agitation produces the same quantity of precipitates (50 g / L of solution) as the magnetic agitation, therefore, both processes have a 100 % efficiency in the reaction, which may be due to the fact that that the same speed is used. This is comparable with Alvear *et al.* (2017) and Yusoff *et al.* (2018), who

also found that the increase of energy in the system by mechanical agitation, induces that the reagents have better distribution in the solution, which causes greater nucleation due to the increase in collisions of the nuclei, thus improving the performance of the reaction and accelerating precipitation.

In this report the sample was dried at 110 °C because with that temperature it was possible to evaporate the residual moisture in less time, however, previous work suggests to calcinate the sample at high temperatures (∼ 600-1200 °C) in order to increase the crystallinity of hydroxyapatite NPs (Meejoo *et al*., 2006), by reducing the amount of water in the structure to increase the intensity and resolution of narrow diffraction peaks. Moreover, this can be associated with mass transport due to the coalescence of hydroxyapatite grains (Kamieniak *et al*., 2017).

On the other hand, Abidi and Murtaza (2013) studied the wet chemical precipitation reaction, finding that the optimum temperature for a stoichiometric ratio of hydroxyapatite NPs is 600 °C. An analogous result to that described above for thermal treatment of this type of NPs was reported by Sanosh *et al*. (2009). They incinerated the hydroxyapatite powders obtained by synthesis using the sol-gel technique, from 65 °C to 800 °C, thereby finding an increase in crystallite size from 18 nm to 61 nm. However, we believe that these high temperatures are not sustainable, since the costs of the process are increased considerably by the concept of energy for heating.

Regarding to the ZP response (Figure 8), the nCF obtained by means of mechanical and magnetic agitation, Mayoral *et al*. (2014) and Ortiz *et al*. (2016) point out that NPs in suspension with charges outside the range ± 30 mV are more stable due to the repulsion by the effect of surface charges, tending to repeal each other which eludes aggregation, however, when the ZP values approach zero, agglomeration of nanoparticles is favored. On the other hand, NPs with a ZP between -10 and +10 mV are considered neutral, while NPs with ZP greater than +30 mV or less than -30 mV are considered strongly cationic and strongly anionic, respectively.

Since most cell walls and membranes are negatively charged, ZP can affect the tendency of NPs to penetrate the membranes, consequently, cationic NPs generally show a greater toxicity associated with the breakdown of the cellular wall (Clogston and Patri, 2011). According to that statement the NPs obtained in this trial will tend to agglomerate, because ZP values of -20 mV to -14 mV were obtained for mechanical

and magnetic agitation respectively, however, Berg *et al*. (2009) stated that this characteristic can be modified if the suspension is adapted, also affecting the dispersion and stability of the suspension.

The results showed that the obtained particles have a negative charge, in a similar way to soil clay, this indicates in turn that nCF would have the capacity to attract other soil nutrients in the form of cations such as Mg^{+2}, Na^{+2}, K^+ and NH_4^+, which supports to retain and maintain these elements on the ground for longer periods improving the nutrient status of plants and crops (Kottegoda *et al*., 2016).

Regarding the toxicity potential of NPs to humans and ecosystems, as nanoparticle size decreases, the surface to volume ratio increases exponentially, which make these particles more reactive and toxic, since by reducing their size, their ability to penetrate plant and animal tissues increases (Sajid *et al*., 2015). Ionic dissolution and particle-induced generation of reactive oxygen species (ROS) are equally a significant mode of action for toxicity, while physical damage to cell membrane are associated to partially soluble Cobalt oxide NPs (Sharan *et al*., 2019). ROS production may lead to an unspecific oxidation of cell membranes, proteins, nucleic acids, and chloroplast pigments. The accumulation of ROS is caused by an imbalance between ROS production and the capacity of the antioxidant system to inactivate them.

In plants, the root growth of radish, rape canola, ryegrass, lettuce, corn, and cucumber species were inhibited upon exposure to 2000 mg/L nano-sized Zn and ZnO. By applying nano-sized Zn (zinc, 35 nm) and ZnO (zinc oxide, 20 nm) the germination of ryegrass and corn was also inhibited (Nhan le *et al*., 2015). In the case of the nCF, no scientific evidence was found on their probable phytotoxicity; on the contrary, nCF are used to immobilize heavy metals in the soil and water, preventing their absorption by plants (Geebelen *et al*., 2002; Yang *et al*., 2016; Guo *et al*., 2019).

According to Bala *et al*. (2014), there is a low possibility that the nCF generates bioaccumulation and / or phytotoxicity, since in its research with chickpea, the HRTEM miracles detected only traces of the material in the treated plants with 1 mg/mL. It is believed that most of the nanoparticle applied was used by the tissues of the plant for their metabolic processes since it was observed an increase in the growth rate of the plant with respect to the control. For this reason, it is considered that the nanoparticles of nCF have great potential in the future of agriculture and more work is needed in this regard.

Conclusions

The present study provides evidence that the preparation of nCF can be feasible by simple low environmental impact procedures of reduced cost, without calcining the sample. Quantitative yields of nCF were achieved by means of wet precipitation using mechanical agitation to control the size of the nanoparticle. The process reported here could be scalable to produce nCF that has commercial potential as a nanofertilizer for the agricultural sector.

References

Abidi, S.S.A., Murtaza, Q. (2013). Synthesis and characterization of nano-hydroxyapatite powder using wet chemical precipitation reaction. *Journal of Materials Science & Technology 30*, 307-310. Doi: 10.1016/j.jmst.2013.10.011

Afshar, A., Ghorbani, M., Ehsani, N., Saeri, M.R., Sorrell, C.C. (2003). Some important factors in the wet precipitation process of hydroxyapatite. *Materials & Design 24*, 197-202. Doi: 10.1016/S0261-3069(03)00003-7

Alvear, D., Galeas, S., Guerrero, V.H., Debut, A. (2017). Synthesis and characterization of magnetite nanoparticles. *Revista Politécnica 39*, 61-66. Doi: 10.1016/S0261-3069(03)00003-7

Angelescu, N., Ungureanu, D.N., Anghelina, F.V. (2011). Synthesis and characterization of hydroxyapatite obtained in different experimental conditions. *Scientific Bulletin of Valahia University Materials and Mechanics 6*, 15-18.

Asif, A.K.M.A.H., Hasan, M.Z. (2018). Application of nanotechnology in modern textiles: A review. *International Journal of Current Engineering and Technology 8*, 227-231. https://doi.org/10.14741/ijcet/v.8.2.5

Azizieh, M., Kokabi, A.H., Abachi, P. (2011). Effect of rotational speed and probe profile on microstructure and hardness of AZ31/Al$_2$O$_3$ nanocomposites fabricated by friction stir processing. *Materials & Design 32*, 2034-2041.

Bakan, F. (2018). Gene delivery by hydroxyapatite and calcium phosphate nanoparticles: A review of novel and recent applications. In Hydroxyapatite-Advances in Composite Nanomaterials. *Biomedical Applications and Its Technological Facets*. InTech.

Bala, N., Dey, A., Das, S., Basu, R., Nandy, P. (2014). Effect of hydroxyapatite nanorod on chickpea (Cicer arietinum) plant growth and its possible use as nano-fertilizer. *Iranian Journal of Plant Physiology 4*, 1061-1069.

Bationo, A., Ngaradoum, D., Youl, S., Lompo, F., Fening, J.O. (Eds.). (2018). *Improving the Profitability, Sustainability and Efficiency of Nutrients through Site Specific Fertilizer Recommendations in West Africa Agro-Ecosystems* (Vol. 1). Springer.

Berg, J.M., Romoser, A., Banerjee, N., Zebda, R., Sayes, C.M. (2009). The relationship between pH and zeta potential of ~30 nm metal oxide nanoparticle suspensions relevant to in vitro toxicological evaluations. *Nanotoxicology 3*, 276-283. Doi: 10.3109/17435390903276941

Clogston, J.D., Patri, A.K. (2011). Zeta potential measurement. Characterization of nanoparticles intended for drug delivery. *Humana Press 2011*, 63-70. Doi:10.1007/978-1-60327-198-1_6

Ferreira, M.A.M., Filipe, J.A. (2018). Nanotechnology applications-The future arrived suddenly. *Computational Approaches in Biomedical Nano-Engineering*, 23-41.

Fihri, A., Len, C., Varma, R.S., Solhy, A. (2017). Hydroxyapatite: A review of syntheses, structure and applications in heterogeneous catalysis. *Coordination Chemistry Reviews 347*, 48-76. Doi: 10.1016/j.ccr.2017.06.009

Geebelen, W., Vangronsveld, J., Adriano, D.C., Carleer, R., Clijsters, H. (2002). Amendment-induced immobilization of lead in a lead-spiked soil: Evidence from phytotoxicity studies. *Water, Air, and Soil Pollution 140*, 261-277. Doi:10.1023/a:1020147901365

Gheisari, H., Karamian, E., Abdellaji, M. (2015). A novel hydroxyapatite-hardistonite nanocomposite ceramic. *Ceramics International 41*, 5967-5975. Doi: 10.1016/j.ceramint.2015.01.033

Guo, H., Jiang, C., Xu, Z., Luo, P., Fu, Z., Zhang, J. (2019). Synthesis of bitter gourd-shaped nanoscaled hydroxyapatite and its adsorption property for heavy metal ions. *Materials Letters 241*, 176-179. Doi: 10.1016/j.matlet.2019.01.028

Guzmán, V.C., Pina, B.C., Munguia, N. (2005). Stoichiometric hydroxyapatite obtained by precipitation and sol gel processes. *Revista Mexicana de Física 51*, 284-293.

Holford, I.C.R. (1997). Soil phosphorus: Its measurement, and its uptake by plants. *Soil Research 35*, 227.

Izumi, F., Takuji I. (2015). *Implementation of the Williamson-Hall and Halder-Wagner Methods into RIETAN-FP*. 2015, 33-38.

Kamieniak, J., Kelly, P.J., Banks, C.E., Doyle, A.M. (2017). Mechanical, pH and thermal stability of mesoporous hydroxyapatite. *Journal of Inorganic and Organometallic Polymers and Materials 28*, 84-91. Doi: 10.1007/s10904-017-0652-3

Kottegoda, N., Madusanka, N., Sandaruwan, C. (2016). Two new plant nutrient nanocomposites based on urea coated hydroxyapatite: Efficacy and plant uptake. *Indian Journal of Agricultural Science 86*, 494-9.

Kottegoda, N., Munaweera, I., Madusanka, N., Karunaratne, V. (2011). A green slow-release fertilizer composition based on urea-modified hydroxyapatite nanoparticles encapsulated wood. *Current Science 101*, 73-78.

Kottegoda, N., Sandaruwan, C., Priyadarshana, G., Siriwardhana, A., Rathnayake, U.A., Berugoda-Arachchige, D.M., Amaratunga, G.A. (2017). Urea-hydroxyapatite nanohybrids for slow release of nitrogen. *American Chemical Society, Nano 11*, 1214-1221. Doi: 10.1021/acsnano.6b07781

Lopez-Bucio, J., de la Vega, O. M., Guevara-García, A., Herrera-Estrella, L. (2000). Enhanced phosphorus uptake in transgenic tobacco plants that overproduce citrate. *Nature Biotechnology 18*, 450.

Ma, M.G. (2012). Hierarchically nanostructured hydroxyapatite: hydrothermal synthesis, morphology control, growth mechanism, and biological activity. *International Journal of Nanomedicine 7*, 1781. Doi: 10.2147/IJN.S29884

Mayoral, J.B., Moreno, A.C., Martínez, E.S.M. (2014). Potencial zeta en la determinación de carga superficial de liposomas. *Latin-American Journal of Physics Education 8*, 19-21.

Meejoo, S., Maneeprakorn, W., Winotai, P. (2006). Phase and thermal stability of nanocrystalline hydroxyapatite prepared via microwave heating. *Thermochemical Acta 447*, 115-120. Doi: 10.1016/j.tca.2006.04.013

Mendoza-Castillo, D.I., Bonilla-Petriciolet, A., Jauregui-Rincon, J. (2016). Statistical analysis and modeling of multicomponent sorption of heavy metals in water using bone char. *Revista Mexicana de Ingenieria Quimica 15*, 525-542.

Mikolajczyk, A., Gajewicz, A., Rasulev, B., Schaeublin, N., Maurer-Gardner, E., Hussain, S., Puzyn, T. (2015). Zeta potential for metal oxide nanoparticles: a predictive model developed by a nano-quantitative structure-property relationship approach. *Chemistry of Materials 27*, 2400-2407. Doi: 10.1021/cm504406a

Montalvo, D., McLaughlin, M.J., Degryse, F. (2015). Efficacy of hydroxyapatite nanoparticles as phosphorus fertilizer in andisols and oxisols. *Soil Science Society of America Journal 79*, 551-558. Doi: 10.2136/sssaj2014.09.0373

Nhan le, V., Ma, C., Rui, Y., Liu, S., Li, X., Xing, B., Liu, L. (2015). Phytotoxic mechanism of nanoparticles: Destruction of chloroplasts and vascular bundles and alteration of nutrient absorption. *Scientific Reports 5*, 11618. Doi:10.1038/srep11618

Okada, M., Matsumoto, T. (2015). Synthesis and modification of apatite nanoparticles for use in dental and medical applications. *Japanese Dental Science Review 51*, 85-95.

Ortiz-Zarama, M.A., Jiménez-Aparicio, A.R., Lourenço, R.V., Amaral-Sobral, P.J., Solorza-Feria, J. (2016). Rheological characterization of solutions of gelatin with bentonite and tannic acid. *Revista Mexicana de Ingeniería Química 15*, 819-830.

Prakash, B., Kujur, A., Yadav, A., Kumar, A., Singh, P.P., Dubey, N.K. (2018). Nanoencapsulation: An efficient technology to boost the antimicrobial potential of plant essential oils in food system. *Food Control 89*, 1-11. Doi: 10.1016/j.foodcont.2018.01.018

Rane, M., Bawskar, M., Rathod, D., Nagaonkar, D., Rai, M. (2015). Influence of calcium phosphate nanoparticles, *Piriformospora indica* and *Glomus mosseae* on growth of *Zea mays*. *Advances in Natural Sciences: Nanoscience and Nanotechnology 6*, 1-8. Doi:10.1088/2043-6262/6/4/045014

Sadat, S.M., Khorasani, M.T., Dinpanah, K.E., Jamshidi, A. (2013). Synthesis methods for nanosized hydroxyapatite with diverse structures. *Acta Biomaterialia 9*, 7591-7621. Doi: 10.1016/j.actbio.2013.04.012.

Sajid, M., Ilyas, M., Basheer, C., Tariq, M., Daud, M., Baig, N., Shehzad, F. (2015). Impact of nanoparticles on human and environment: review of toxicity factors, exposures, control strategies, and future prospects. *Environmental Science and Pollution Research 22*, 4122-4143.

Salgado-Delgado, A.M., Vargas-Galarza, Z., Salgado-Delgado, R., Garcia-Hernandez, E., Hernandez-Diaz, W.N., Rubio-Rosas, E., Salgado-Rodriguez, R. (2016). Morphological and thermal characterization of a high porous composite of biomaterial phema-chitosan-ceramic (hydroxyapatite). *Revista Mexicana de Ingeniería Química 15*, 625-632.

Salimi, M.N., Bridson, R.H., Grover, L.M., Leeke, G.A. (2012). Effect of processing conditions on the formation of hydroxyapatite nanoparticles. *Powder Technology 218*, 109-118. Doi: 10.1016/j.powtec.2011.11.049

Sanosh, K.P., Chu, M.C., Balakrishnan, A., Kim, T.N., Cho, S.J. (2009). Preparation and characterization of nano-hydroxyapatite powder using sol-gel technique. *Bulletin of Materials Science 32*, 465-470.

Sattary, M., Rafienia, M., Kazemi, M., Salehi, H., Mahmoudzadeh, M. (2019). Promoting effect of nano hydroxyapatite and vitamin D3 on the osteogenic differentiation of human adipose-derived stem cells in polycaprolactone/gelatin scaffold for bone tissue engineering. *Material Science and Engineering C 97*, 141-155. Doi: 10.1016/j.msec.2018.12.030

Saxena, M., Okram, G.S. (2018). Zeta potential study of Sb_2S_3 nanoparticles synthesized by a facile polyol method in various surfactants. In *AIP Conference Proceedings 1953*, 030092. AIP Publishing. Doi: 10.1063/1.5032427.

Sharan, A., Nara, S. (2019). *Phytotoxic Properties of Zinc and Cobalt Oxide Nanoparticles in Algaes. In Nanomaterials in Plants, Algae and Microorganisms*. Academic Press. 1-22.

Sunandhakumari, V.J., Vidhyadharan, A.K., Alim, A., Kumar, D., Ravindran, J., Krishna, A., Prasad, M. (2018). Fabrication and *in vitro* characterization of bioactive glass/nano hydroxyapatite reinforced electrospun poly(epsilon-caprolactone) composite membranes for guided tissue regeneration. *Bioengineering (Basel) 5*. Doi:10.3390/bioengineering5030054

Velasco-Rodríguez, V., Cornejo-Mazón, M., Flores-Flores, J.O., Gutiérrez-López, G.F., Hernández-Sánchez, H. (2012). Preparation and properties of alpha-lipoic acid-loaded chitosan nanoparticles. *Revista Mexicana de Ingeniería Química 11*, 155-161.

Yang, Y., Chawla, A., Zhang, J., Esa, A., Jang, H.L., Khademhosseini, A. (2019). Applications of nanotechnology for regenerative medicine; healing tissues at the nanoscale. In *Principles of Regenerative Medicine*. Academic Press 485-504. Doi: 10.1016/B978-0-12-809880-6.00029-1

Yang, Y., Xu, S., Xu, G., Liu, R., Xu, A., Chen, S., Wu, L. (2019). Effects of ionic strength on physicochemical properties and toxicity

of silver nanoparticles. *Science of the Total Environment 647*, 1088-1096.

Yang, Z., Fang, Z., Tsang, P.E., Fang, J., Zhao, D. (2016). In situ remediation and phytotoxicity assessment of lead-contaminated soil by biochar-supported nHAP. *Journal of Environmental Management 182*, 247-251. Doi: 10.1016/j.jenvman.2016.07.079

Yelten, A., Yilmaz, S. (2016). Various parameters affecting the synthesis of the hydroxyapatite powders by the wet chemical precipitation technique. *Materials Today: Proceedings 3*, 2869-2876. Doi: 10.1016/j.matpr.2016.07.006

Yusoff, A.H.M., Salimi, M.N., Jamlos, M.F. (2018). Critical parametric study on final size of magnetite nanoparticles. *IOP Conference Series: Materials Science and Engineering 318*, 2-20. Doi: 10.1088/1757-899X/318/1/012020

https://www.chromspheres.com/nano-hydroxyapatite-powder/ Accessed: 01 March 2019